Lawrence Berkeley National Laboratory

Title
Interface-engineered hole doping in Sr2IrO4/LaNiO3 heterostructure

Authors
Wen, Fangdi
Liu, Xiaoran
Zhang, Qinghua
et al.

PAPER • OPEN ACCESS

Interface-engineered hole doping in Sr_2IrO_4/$LaNiO_3$ heterostructure

New Journal of Physics

The open access journal at the forefront of physics

PAPER

Interface-engineered hole doping in Sr$_2$IrO$_4$/LaNiO$_3$ heterostructure

Fangdi Wen[1] , Xiaoran Liu[1], Qinghua Zhang[2], M Kareev[1], B Pal[1], Yanwei Cao[3], J W Freeland[4], A T N'Diaye[5], P Shafer[5], E Arenholz[5], Lin Gu[2] and J Chakhalian[1]

1   Department of Physics and Astronomy, Rutgers University, Piscataway, NJ 08854, United States of America
2   Beijing National Laboratory for Condensed-Matter Physics and Institute of Physics, Chinese Academy of Sciences, Beijing 100190, People's Republic of China
3   Ningbo Institute of Materials Technology and Engineering, Chinese Academy of Sciences, Ningbo, Zhejiang 315201, People's Republic of China
4   Advanced Photon Source, Argonne National Laboratory, Argonne, IL 60439, United States of America
5   Advanced Light Source, Lawrence Berkeley National Laboratory, Berkeley, CA 94720, United States of America

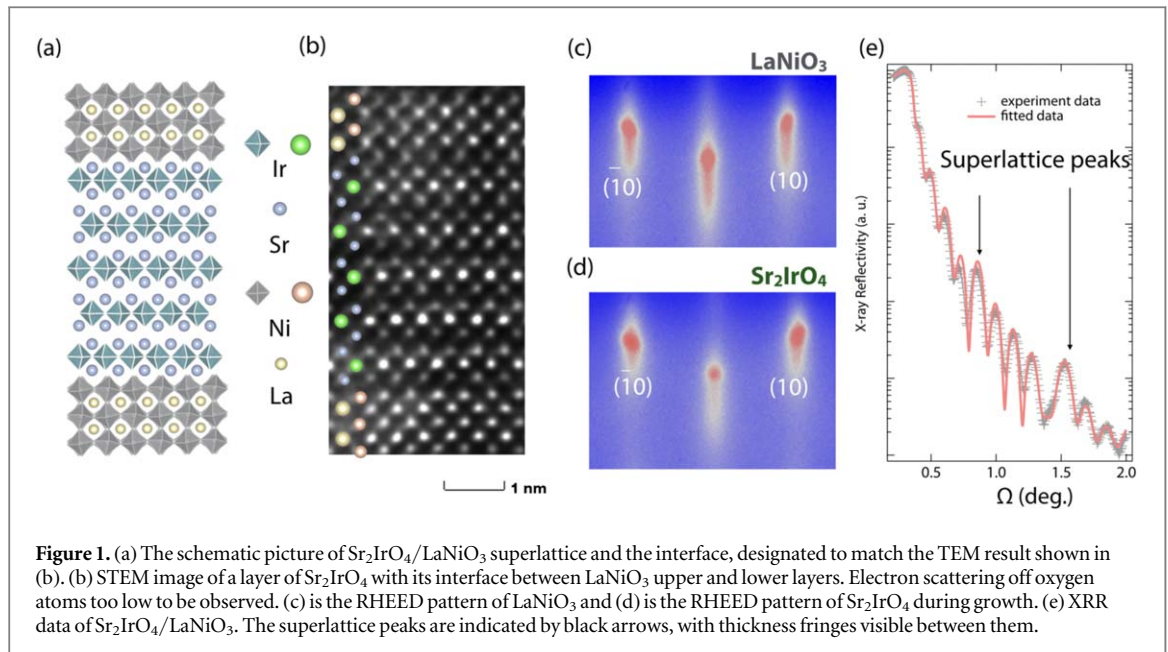E-mail: fw113@physics.rutgers.edu and xiaoran.liu@rutgers.edu

Abstract

The relativistic Mott insulator Sr$_2$IrO$_4$ driven by large spin–orbit interaction is known for the $J_{eff} = 1/2$ antiferromagnetic state which closely resembles the electronic structure of parent compounds of superconducting cuprates. Here, we report the realization of hole-doped Sr$_2$IrO$_4$ by means of interfacial charge transfer in Sr$_2$IrO$_4$/LaNiO$_3$ heterostructures. X-ray photoelectron spectroscopy on Ir $4f$ edge along with the x-ray absorption spectroscopy at Ni L_2 edge confirmed that $5d$ electrons from Ir sites are transferred onto Ni sites, leading to markedly electronic reconstruction at the interface. Although the Sr$_2$IrO$_4$/LaNiO$_3$ heterostructure remains non-metallic, we reveal that the transport behavior is no longer described by the Mott variable range hopping mode, but by the Efros–Shklovskii model. These findings highlight a powerful utility of interfaces to realize emerging electronic states of the Ruddlesden–Popper phases of Ir-based oxides.

1. Introduction

Transition metal oxides (TMOs) with a partially filled d-shell often host strongly correlated carriers and exhibit unique physical properties due to the intertwined lattice, charge, orbital and spin degrees of freedom [1]. In $3d$ TMOs, since the crystal field (CF) splitting Δ_{CF} is approximately an order of magnitude larger than the intrinsic spin–orbit coupling (SOC) λ, the effect of SOC is usually neglected in the determination of the ground state. However, in $4d$ and $5d$ TMOs, the enhancement of λ makes it become comparable to Δ_{CF}. As the outcome of the competing interactions dominated by SOC, a large number of unusual quantum states, including topological insulators [2], quantum spin liquids [3], Weyl semimetals [4], and Kitaev materials [5] have been recently predicted. In this category, Sr$_2$IrO$_4$ is one of the prototypical examples of materials known as the relativistic Mott insulators. Naively, due to the spatially extended $5d$ orbitals and the decreased on-site Coulomb repulsion, a metallic ground state is naturally expected in this compound. Contrary to the expectation, Sr$_2$IrO$_4$ is antiferromagnetic insulator [6]. To explain the discrepancy, the proposed physical picture suggests that the degeneracy of the Ir $5d$ levels is first lifted by the CF splitting while the strong SOC further splits the t_{2g} bands into fully occupied $J_{eff} = 3/2$ subbands and a half-filled $J_{eff} = 1/2$ subband. Additionally, the on-site Coulomb interaction further splits the $J_{eff} = 1/2$ band into an upper Hubbard band (UHB) and a lower Hubbard band (LHB), realizing the spin-orbit assisted Mott ground state [7, 8].

Based on this picture, a strong similarity between Sr$_2$IrO$_4$ and the parent compounds of high T_c cuprates has been highlighted in various experiments. Specifically, Sr$_2$IrO$_4$ crystallizes in the K$_2$NiF$_4$-type structure and is an antiferromagnetic insulator with the magnetic transition temperature $T_c \sim 240$ K [8, 9]. Resonant inelastic x-ray scattering experiments revealed that the magnetic excitations of Sr$_2$IrO$_4$ on the square lattice can be well described within an antiferromagnetic Heisenberg model [10] akin to the parent compounds of cuprates. Furthermore, it has been proposed that upon hole and electron doping, this material can potentially host a high T_c superconducting state [11–13].

Figure 1. (a) The schematic picture of Sr_2IrO_4/$LaNiO_3$ superlattice and the interface, designated to match the TEM result shown in (b). (b) STEM image of a layer of Sr_2IrO_4 with its interface between $LaNiO_3$ upper and lower layers. Electron scattering off oxygen atoms too low to be observed. (c) is the RHEED pattern of $LaNiO_3$ and (d) is the RHEED pattern of Sr_2IrO_4 during growth. (e) XRR data of Sr_2IrO_4/$LaNiO_3$. The superlattice peaks are indicated by black arrows, with thickness fringes visible between them.

Recent measurements have provided many evidences for the possible superconducting hidden phase in Sr_2IrO_4 [14–18]. Despite the early encouraging progress, to date, there is no report on superconducting behavior in doped Sr_2IrO_4 [19–22]. Naturally, one of the possible reasons could be that the degree of doping has not reached the critical value from which the superconducting state can emerge. However, there has been chemical doping reaching the level of the theory prediction (around ∼12% or more), but the superconducting phase is yet to be found [13, 15, 16, 21, 22]. Considering that the high chemical doping level might, on the other hand, also affect many crytallographic properties of the system, searching for alternative ways to realize such a high doping in Sr_2IrO_4 without atoms replacement might be vital to identify the hidden superconducting phase with iridates.

In this letter, we report on creating high hole doping of Sr_2IrO_4 by virtue of engineering a heteroepitaxial interface composed of Sr_2IrO_4 and $LaNiO_3$ ultra-thin layers. Scanning transmission electron microscopy (STEM) and x-ray reflectivity (XRR) results confirm high quality, good crystallinity, well-formed interfaces and expected periodicity of the heterostructures. Photoelectron spectroscopy data (XPS) and x-ray absorption spectra (XAS) reveal distinct charge modulations at the interface, leading to electron transfer from Ir to Ni sites across the interfaces. X-ray linear dichroism (XLD) studies have revealed that the charge redistribution lifts the orbital degeneration in Ni^{2+}, and therefore created the Ni^{2+} ($S = 1$) and Ir^{5+} ($J_{eff} = 0$) electronic configurations at the interface. Although the heterostructure remains insulating, we found that the transport behavior is no longer described by the Mott variable range hopping (VRH) model, but by the Efros–Shklovskii (E–S) model.

2. Experimental section

High-quality Sr_2IrO_4/$LaNiO_3$ superlattices were epitaxially synthesized on (001) oriented $SrTiO_3$ substrate by pulsed laser deposition (KrF excimer laser, $\Lambda = 248$ nm) with substrate temperature of ∼690 °C and oxygen pressure of 10 mTorr. Targets were ablated at the laser frequency of 2 Hz and fluency of 1–4 J cm^{-2}. The layer-by-layer growth was monitored by *in situ* high-pressure reflection high-energy election diffraction (RHEED).

The crystallinity and epitaxy of the sample has been verified by several methods. First, the samples have been investigated by STEM (see figure 1(b)). As seen, within the $LaNiO_3$ layers, the La distribution shows a typical perovskite structure. In the Sr_2IrO_4, two atomic planes of SrO are observed between each layer of IrO_2 in accord with the expected layered-perovskite structure. To avoid extra conducting channels, the electron acceptor $LaNiO_3$ layers were designed thin enough (∼2 unit cells) to be insulating [23]. Sharp interfaces between Sr_2IrO_4 and $LaNiO_3$ resulting from the layer-by-layer structure of the heterostructure are also evident from the STEM images. The STEM result is in a good agreement with the *in situ* RHEED measurements for both Sr_2IrO_4 and $LaNiO_3$ layers (see figure 1(c) and (d)). Furthermore, the XRR measurement confirms the superlattice structure and allow to estimate the total film thickness, as shown in figure 1(e). The total thickness obtained from the fitting result is ∼30.768 ($\pm$0.13) nm while the thickness of each individual layer (one layer of Sr_2IrO_4 + one layer of $LaNiO_3$) is ∼6.221 ($\pm$0.014) nm.

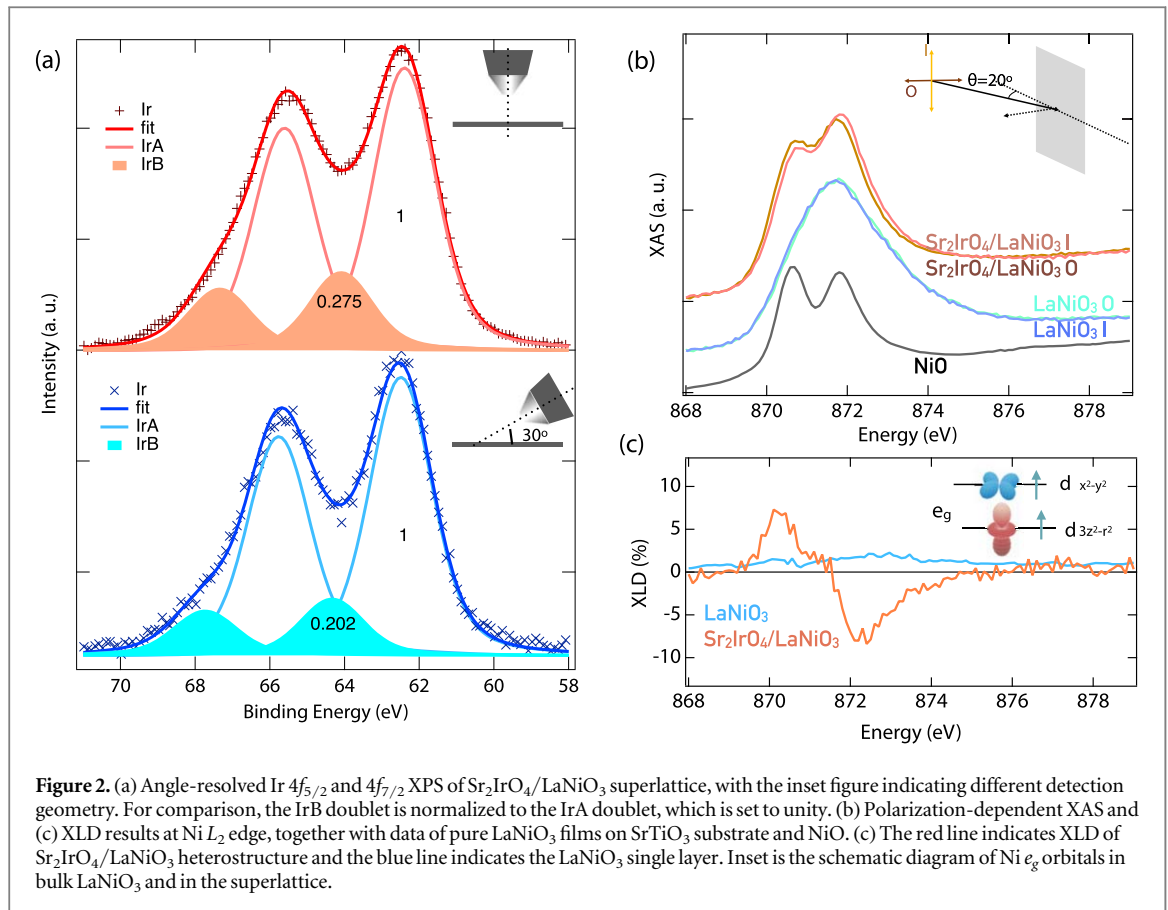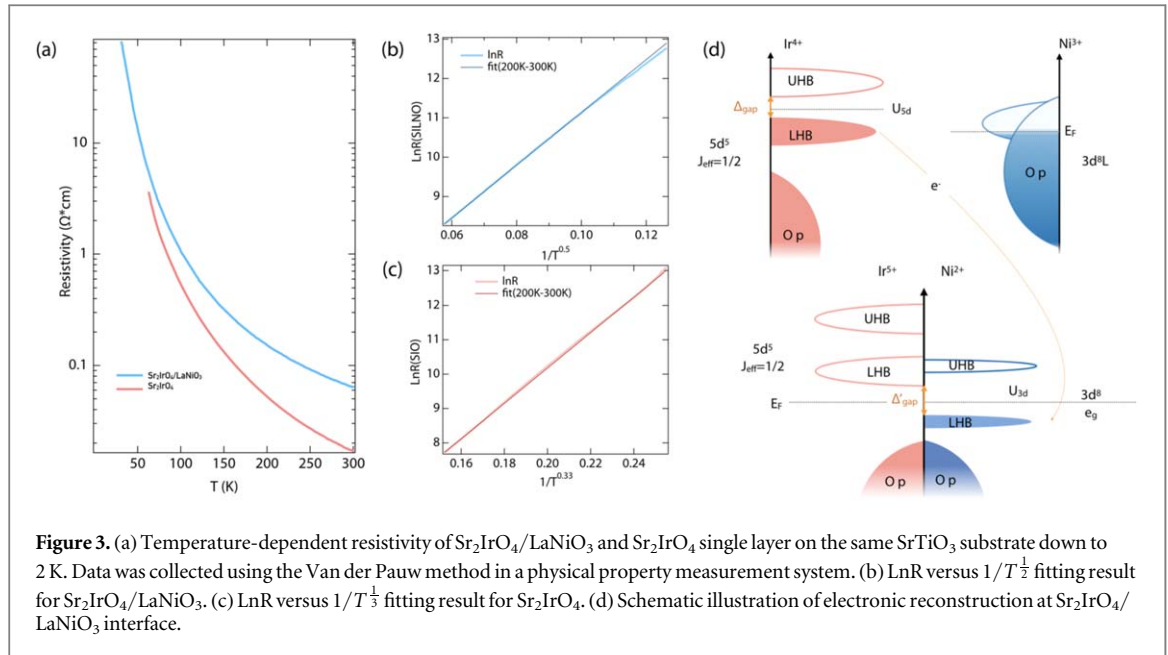**Figure 2.** (a) Angle-resolved Ir $4f_{5/2}$ and $4f_{7/2}$ XPS of $Sr_2IrO_4/LaNiO_3$ superlattice, with the inset figure indicating different detection geometry. For comparison, the IrB doublet is normalized to the IrA doublet, which is set to unity. (b) Polarization-dependent XAS and (c) XLD results at Ni L_2 edge, together with data of pure $LaNiO_3$ films on $SrTiO_3$ substrate and NiO. (c) The red line indicates XLD of $Sr_2IrO_4/LaNiO_3$ heterostructure and the blue line indicates the $LaNiO_3$ single layer. Inset is the schematic diagram of Ni e_g orbitals in bulk $LaNiO_3$ and in the superlattice.

Next, to understand the electronic structure associated with the Ir charge state at the $Sr_2IrO_4/LaNiO_3$ interfaces, we carried out a set of XPS measurements with different detection angle. Figure 2(a) shows the Ir $4f$ core level spectrum of the superlattice. From the direct fitting of the spectral shape, one can see that the Ir $4f$ envelope contains two doublet contributions. Specifically, the main doublet appearing at binding energy 62.3 and 65.6 eV represents the Ir^{4+} states which are expected for the stoichiometric undoped system (IrA). There is also another doublet contribution (IrB) with binding energy close to 64 and 67.3 eV, which can result from the formation of Ir^{5+}, or accompanied satellite peaks of Ir^{4+} [24–27]. In order to prove the existence of Ir^{5+}, angle-resolved XPS was conducted with two different detection angles. By changing the detection geometry, the XPS can show signals with different probing depth. If the IrB doublet is purely the satellite peaks, the relative intensity to the main doublet IrA should be a fixed value at different detection angle. However, there is a clear variation of IrB relative intensity as the detector is changed from normal to grazing position. This observation confirms the presence of Ir^{5+} in Sr_2IrO_4 layers at the interfacial region.

Next, we turn to investigate the charge distribution on Ni in the vicinity of the interface by XAS at the Ni L_2 edge. As seen in a typical scan depicted in figure 2(b) there is a clear double peak structure at the L_2 edge in the superlattice with either horizontal- or vertical-polarized x-rays (orange curve). This observation is in sharp contrast to the reference $LaNiO_3$ sample with pure Ni^{3+}, confirming the presence of Ni^{2+} due to the charge transfer. By fitting the XAS result of the superlattices with respect to the pure Ni^{3+} and Ni^{2+} reference samples, the contribution of Ni^{2+} is ∼70%, which indicates a large amount charge transfer happening at the interfaces.

Soft x-ray absorption with linearly polarized light or XLD allows for further insight into the orbital occupation of the Ni^{2+}. Experimentally, the XLD is defined as the difference between absorption spectra measured with horizontally polarized light (O) where the polarization points out of the plane, and in-plane polarized light (I) with polarization in the plane, or I_O–I_I. As shown in figure 2(c), in the undoped $LaNiO_3$ layer (before charge transfer) Ni^{3+} is in $3d^7$ state with the t_{2g} band fully occupied and e_g band occupied by one electron. After electron transfer nickel ions shift the Ni valence state down towards Ni^{2+} with two electrons occupying the e_g orbitals. In our experimental setup, out-of-plane polarized x-rays probe the empty out-of-plane orbitals ($d_{3z^2-r^2}$) while in-plane polarized light senses primarily $d_{x^2-y^2}$ orbital character. The observed XLD signal can be attributed to the difference in orbital occupation of $d_{3z^2-r^2}$ versus $d_{x^2-y^2}$ orbitals. From the XAS data shown in figure 2(b) and the XLD data shown in figure 2(c), one can see that the absorption of photons with horizontal polarization (O) is shifted lower in energy relative to photons with vertical polarization (I) shifted to a higher energy. This result implies that the interface imposes a sub-band splitting of ∼0.1 eV $\triangle e_g$ which lowers the Ni $d_{3z^2-r^2}$ and lifts the $d_{x^2-y^2}$ orbital states (see figure 2(c) inset). Further, the integrated XLD

Figure 3. (a) Temperature-dependent resistivity of $Sr_2IrO_4/LaNiO_3$ and Sr_2IrO_4 single layer on the same $SrTiO_3$ substrate down to 2 K. Data was collected using the Van der Pauw method in a physical property measurement system. (b) LnR versus $1/T^{\frac{1}{2}}$ fitting result for $Sr_2IrO_4/LaNiO_3$. (c) LnR versus $1/T^{\frac{1}{3}}$ fitting result for Sr_2IrO_4. (d) Schematic illustration of electronic reconstruction at $Sr_2IrO_4/LaNiO_3$ interface.

area is close to zero, suggesting that both orbitals are equally occupied [28–30]. In short, the XAS/XLD measurements confirm the electrons transferred from Ir to Ni sites. This leads to (i) formation of Ni^{2+} with high spin $S = 1$ configuration at the interface, and (ii) split of the Ni e_g band into two sub-bands with predominant $d_{x^2-y^2}$ orbital and $d_{3z^2-r^2}$ orbital character.

After establishing the orbital reconstructions at the interfaces, a critical question yet remains: Has the hole doping of Sr_2IrO_4 lead to the formation of a metallic phase? To investigate this issue, the temperature dependence of resistivity on both the superlattice and undoped Sr_2IrO_4 thin film were carried out from 300 K down to 2 K. As shown in figure 3(a), an overall insulating behavior still persists in the superlattice, with the magnitude of resistivity exceeding the measurable limit at ~30 K. Note that the resistivity of $Sr_2IrO_4/LaNiO_3$ superlattice is much higher than that in a purely confined two unit cells $LaNiO_3$ layer, and in another e-doped $LaNiO_3$ superlattices, $LaNiO_3/La_2CuO_4$. This may indicate that apart from quantum confinement, other effects such as charge disproportionation in the nickelate layers may also occur as a result of the interfacial charge doping, leading to higher resistivity [31]. By fitting the transport result with different VRH models: $\sigma = \sigma_0 \exp\left\{\left(\frac{T_0}{T}\right)^{1/(\beta+1)}\right\}$ under all different β selection ($\beta = 0, 1, 2, 3$) with the same temperature range, we found out that the best fitting model for the doped and undoped system are different. In undoped Sr_2IrO_4, it fits well with $\beta = 2$, indicating a conventional 2D Mott VRH model (figure 3(c)). This has also been observed in the undoped Sr_2IrO_4 from other groups, assuming that the band gap in the system is smaller than thermal activation ($\Delta_{gap} < k_BT$) [22, 32, 33]. On the other hand, for doped Sr_2IrO_4, the best fitting result comes from the $\beta = 1$ case, which is the E–S VRH model (figure 3(b)). Within the Mott–Hubbard model, the density of states in the vicinity of the Fermi level is finite. However, the situation is different in the E–S VRH model, where a Coulomb gap is opened as a result of interactions between localized electrons, leading to a small jump in density of states near the Fermi level. In this case, a Coulomb gap larger than the thermal activation ($\Delta_{gap} > k_BT$) is opened, and the electrons become more localized after hole doping [34]. In the following, we propose a possible scenario to interpret the electronic reconstruction at $Sr_2IrO_4/LaNiO_3$ interface.

As seen in figure 3(d), bulk $LaNiO_3$ is a negative charge-transfer metal, whose Fermi surface lies in hybridized O 2p and Ni 3d state [35, 36]. Due to the strong O–Ni hybridization, the electronic structure of bulk $LaNiO_3$ is best represented as a mixture of $3d^7$, $3d^8\underline{L}$ and $3d^9\underline{LL}$ ($\underline{L}$ is a hole on oxygen 2p orbital) [37]. For Sr_2IrO_4, the Fermi surface is between the LHB and UHB of the $J_{eff} = 1/2$ band. Driven by the chemical potential difference across the $Sr_2IrO_4/LaNiO_3$ interfaces, electrons are transferred from the Ir to the Ni site. Ir^{4+} becomes Ir^{5+} with the fully occupied $J_{eff} = 3/2$ band still below the Fermi level. The electron then can fill the hole on oxygens, and reduce the degree of hybridization by lowering the oxygen p orbitals and split the Ni 3d band due to the on-site Coulomb repulsion, U. Since on Ni U is rather large (~4 eV), splitting of the Ni e_g band will likely push the Ni up Hubbard band (UHB) away from the Fermi level and above the Ir $J_{eff} = 1/2$ low Hubbard band (LHB) bands. As the result, the band gap at the interface is determined by the energy interval between the top of Ni e_g LHB and the bottom of Ir $J_{eff} = 1/2$ LHB.

3. Conclusion

In conclusion, by growing a $Sr_2IrO_4/LaNiO_3$ superlattice, we have achieved hole doping of Sr_2IrO_4 without detrimental effects of chemical disorder. XPS and XAS measurements confirm a charge transfer from Ir^{4+} to Ni^{3+}, resulting in a markedly fraction of Ir^{5+} and Ni^{2+}. The latter is accompanied by a lifting of degeneracy in the Ni e_g orbitals, with the $d_{3z^2-r^2}$ orbital 0.1 eV lower than $d_{x^2-y^2}$, as evidenced by XLD measurements. Hole doping via the interface enhanced the on-site Coulomb interaction and enlarged the magnitude of the band gap in the $Sr_2IrO_4/LaNiO_3$ heterostructure compared to a Sr_2IrO_4 single layer. These results explore the phase diagram of Sr_2IrO_4 on the hole-doping side, and pave an alternative way towards the modification of carrier concentration in the relativistic Mott insulator Sr_2IrO_4.

Acknowledgments

ORCID iDs

Fangdi Wen ⓘ https://orcid.org/0000-0003-2314-8561

References

[1] Imada M, Fujimori A and Tokura Y 1998 *Rev. Mod. Phys.* **70** 1039
[2] Uchida M and Kawasaki M 2018 *J. Phys. D: Appl. Phys.* **14** 51
[3] Balents L 2010 *Nature* **464** 199–208
[4] Rau J G, Lee E K H and Kee H Y 2016 *Annu. Rev. Condens. Matter Phys.* **7** 195–221
[5] Witczak-Krempa W, Chen G, Kim Y B and Balents L 2014 *Annu. Rev. Condens. Matter Phys.* **5** 57–82
[6] Chikara S, Korneta O, Crummett W P, DeLong L E, Schlottmann P and Cao G 2009 *Phys. Rev. B* **80** 140407
[7] Kim B *et al* 2008 *Phys. Rev. Lett.* **101** 076402
[8] Kim B, Ohsumi H, Komesu T, Sakai S, Morita T, Takagi H and Arima T H 2009 *Science* **323** 1329–32
[9] Cao G, Bolivar J, McCall S, Crow J and Guertin R 1998 *Phys. Rev. B* **57** R11039
[10] Kim J *et al* 2012 *Phys. Rev. Lett.* **108** 177003
[11] Wang F and Senthil T 2011 *Phys. Rev. Lett.* **106** 136402
[12] Meng Z Y, Kim Y B and Kee H-Y 2014 *Phys. Rev. Lett.* **113** 177003
[13] Watanabe H, Shirakawa T and Yunoki S 2013 *Phys. Rev. Lett.* **110** 027002
[14] Yan Y, Ren M, Xu H, Xie B, Tao R, Choi H, Lee N, Choi Y, Zhang T and Feng D 2015 *Phys. Rev. X* **5** 041018
[15] Cao Y *et al* 2016 *Nat. Commun.* **7** 11367
[16] Zhao L, Torchinsky D H, Chu H, Ivanov V, Lifshitz R, Flint R, Qi T, Cao G and Hsieh D 2016 *Nat. Phys.* **12** 32–6
[17] de la Torre A *et al* 2015 *Phys. Rev. Lett.* **115** 176402
[18] Kim Y K, Sung N H, Denlinger J D and Kim B J 2016 *Nat. Phys.* **12** 37
[19] Chen X, Schmehr J L, Islam Z, Porter Z, Zoghlin E, Finkelstein K, Ruff J P and Wilson S D 2018 *Nat. Commun.* **9** 103
[20] Korneta O, Qi T, Chikara S, Parkin S, De Long L, Schlottmann P and Cao G 2010 *Phys. Rev. B* **82** 115117
[21] Ravichandran J, Serrao C R, Efetov D K, Yi D, Oh Y S, Cheong S-W, Ramesh R and Kim P 2016 *J. Phys.: Condens. Matter* **28** 505304
[22] Li M, Liu Z, Yang H, Zhao J, Yao Q, Fan C, Liu J, Gao B, Shen D and Xie X 2015 *Chin. Phys. Lett.* **32** 057402
[23] Golalikhani M *et al* 2018 *Nat. Commun.* **9** 2206
[24] Banerjee A, Sannigrahi J, Giri S and Majumdar S 2017 *Phys. Rev. B* **96** 224426
[25] Kumar H, Dhaka R and Pramanik A 2017 *Phys. Rev. B* **95** 054415
[26] Zhu W K, Wang M, Seradjeh B, Yang F and Zhang S 2014 *Phys. Rev. B* **90** 054419
[27] Liu X, Cao Y, Pal B, Middey S, Kareev M, Choi Y, Shafer P, Haskel D, Arenholz E and Chakhalian J 2017 *Phys. Rev. M* **1** 075004
[28] Cui B, Song C, Li F, Wang G, Mao H, Peng J, Zeng F and Pan F 2014 *Sci. Rep.* **4** 4206
[29] Pesquera D, Herranz G, Barla A, Pellegrin E, Bondino F, Magnano E, Sánchez F and Fontcuberta J 2012 *Nat. Commun.* **3** 1189
[30] Chakhalian J *et al* 2011 *Phys. Rev. Lett.* **107** 116805
[31] Wrobel F *et al* 2018 *Phys. Rev. Mater.* **2** 035001
[32] Lu C, Quindeau A, Deniz H, Preziosi D, Hesse D and Alexe M 2014 *Appl. Phys. Lett.* **105** 082407
[33] Mott N F 1969 *Phil. Mag.* **19** 835–52
[34] Efros A L and Shklovskii B I 1975 *J. Phys. C: Solid State Physics* **8** 4
[35] Dobin A Y, Nikolaev K, Krivorotov I, Wentzcovitch R, Dahlberg E D and Goldman A 2003 *Phys. Rev. B* **68** 113408
[36] Guo H *et al* 2018 *Nat. Commun.* **9** 2206
[37] Golalikhani M *et al* 2018 *Nat. Commun.* **9** 2206